EurJOC
European Journal of Organic Chemistry

Research Article
doi.org/10.1002/ejoc.202500035

Chemistry Europe
European Chemical Societies Publishing

www.eurjoc.org

Amphiphilic Fluoro-Functionalized Cellulosic Materials: Synthesis, Characterization, and Organic Dye Adsorption Properties

Davide Ricci, Andrea Maio, Christian Jahns, Elena Piacenza, Delia Francesca Chillura Martino, Roberto Scaffaro, Margit Schulze, Andrea Pace, Carla Rizzo,* and Ivana Pibiri

The growing interest toward biopolymers application in amphiphilic conditions prompts one to explore the preparation of fluorinated cellulosic materials. Cellulose (CE) and carboxymethylcellulose (CMC) are functionalized with highly fluorinated pendants, through a nucleophilic aromatic substitution on 3-pentadecafluoroheptyl-5-pentafluorophenyl-1,2,4-oxadiazole (FOX) leading to the corresponding fluorinated biopolymers CE-FOX and CMC-FOX. Structural and thermal stability confirm covalent attachment of the fluorinated moiety onto the cellulosic skeleton and highlighted an interesting 2D texture of the CMC-FOX material. Hybrid and amphiphilic features of CE-FOX and CMC-FOX, are confirmed by water and oil contact angle measurements. Applications as adsorbent material for organic contaminants from an aqueous solution are tested by previously incorporating the functional biopolymer into sodium alginate (SA) hydrogel beads. Rhodamine B (RhB) is used as a model wastewater pollutant. Fluoro-functionalization led to a three- to eightfold increase in the dye-removal efficiency of the SA-incorporated biopolymer with respect to the corresponding non-fluorinated material (from 11% to 48% for SA/CE vs SA/CE-FOX beads and from 11% to 94% for SA/CMC vs SA/CMC-FOX beads). Recyclability tests show good residual performance of SA/CMC-FOX beads after seven desorption/reuse cycles opening the way to more sustainable adsorbing processes for the removal of emerging pollutants from contaminated water.

1. Introduction

Freshwater is a critical resource for the planet and biopolymers are recently emerging as good adsorbents in the field of sustainable wastewater remediation.[1] However, their high hydrophilicity limits their use for the adsorption of organic molecules. Therefore, the modification of hydrophilic biopolymers with hydrophobic molecules can overcome this issue, leading to either amphiphilic or hydrophobic materials, depending on the degree of functionalization.[2]

Due to their natural source, continuous regeneration, and abundant availability, biopolymers are the most promising substitutes for synthetic polymers, allowing a reduction in their negative impact on the planet.[3] Vegetal biopolymers occur naturally in all plants, where they compose the outer and inner cell walls. Indeed, one of the main components that make up natural plant fibers is cellulose (CE), consisting of 1,4-β-glycosidic connected glucose molecules. CE is the most abundant biopolymer in the world, with 1.5×10^{12} tons of annual biomass production. It is estimated that CE can hardly be depleted even with an increasing demand for the production of environmentally friendly materials and products.[4] Polymers based on cellulose are highly desirable, showing robust mechanical properties, predictable and tunable biodegradability, and overall sustainability.

To address issues of low solubility, thermal processability, and polymer compatibility, cellulose is often modified through esterification, etherification, oxidation, or other chemical processes.[5] A typical cellulose modification consists of the esterification of CE hydroxyl groups with carboxylic anhydrides under acidic catalysis producing various degrees of functionalization, although introducing a potentially hydrolizable moiety.[6]

Another typical cellulose modification involves the etherification of CE hydroxyl groups with chloroacetic acid, producing carboxymethyl cellulose (CMC). Due to the presence of carboxylic moieties, CMC is more hydrophilic and soluble in water than cellulose, can form gels and emulsions, and can be used for biomedical and pharmaceutical applications as well as in the textile and food industry.[7]

D. Ricci, C. Jahns, E. Piacenza, D. F. Chillura Martino, A. Pace, C. Rizzo, I. Pibiri
Department of Biological
Chemical and Pharmaceutical Sciences and Technologies
Section of Chemistry
University of Palermo
Viale delle Scienze, Ed. 17, 90128 Palermo, Italy
E-mail: carla.rizzo03@unipa.it

A. Maio, R. Scaffaro
Department of Engineering
University of Palermo
Viale delle Scienze – Parco d'Orleans II, Ed. 6, 90128 Palermo, Italy

C. Jahns, M. Schulze
Department of Natural Sciences
Bonn-Rhein-Sieg University of Applied Sciences
von-Liebig-Straße 20, 53359 Rheinbach, Germany

Supporting information for this article is available on the WWW under https://doi.org/10.1002/ejoc.202500035

Research Article
doi.org/10.1002/ejoc.202500035

Among different types of polymer functionalization, hydrophobic or superhydrophobic artificial coatings are highly useful in various applications, such for water remediation, oil/water separation, or for the manufacturing of self-cleaning, anti-fouling, anti-corrosion, or anti-viral/anti-bacterial material.[8] In this context, the functionalizing of polymers with fluorinated compounds has been widely used to introduce peculiar wetting behavior and properties, such as low surface energy, high chemical stability, and hydrophobicity.[9] In this context, due to the wide range of applications of fluorinated polymers,[10] the fluoro-functionalization, that is. the polymer functionalization with fluorinated compounds, of biopolymers represents a promising strategy to substitute oil-derived fluoropolymers.

Recently, bio-based materials are applied on various surfaces to develop hydrophobic coatings with longer durability by lowering the surface energy and increasing the surface roughness.[11] Additionally, highly fluorinated biopolymers have been used as coatings for ^{19}F magnetic resonance imaging.[12] Furthermore, CE has been recently esterified with a multibranched fluorinated carboxylic acid, forming either flat and transparent or rough and translucent films depending on the cellulose/fluorinated moiety ratio, which affected the mechanical behavior from rigid to ductile and soft films.[13] As for the fluoro-functionalization approach, some eco-friendly methodology was developed to functionalize cellulose nanofibers (CNFs) with fluoroalkylic chains, obtaining waterproof paper with microbial resistance properties.[14]

A potential application of fluorinated biopolymers could be envisaged in the field of ultrafiltration membranes that are usually made of hydrophobic polymers.[15] However, high hydrophobicity could limit the water permeation flux or induce fouling, two major obstacles to the development of membrane technology.[16] To prevent these issues, a partial hydrophobic functionalization of biopolymers could lead to either zwitterionic or amphiphilic materials.[17] Alternatively, to maintain anti-fouling properties, hydrophilic polymers could be blended with fluorinated polymers.[18] Indeed, a low surface energy, hydrophobicity, and oleophobicity of fluoropolymers presenting strong chemical and thermal stability makes them an attractive component for use in amphiphilic networks.[19] Recently, several polymeric materials containing fluorophilic perfluoropolyether urethane dimethacrylate and zwitterionic carboxybetaine methacrylate were anchored to chemically functionalized substrates by grafting through polymerization.[20]

Functionalized biopolymers containing ionogenic groups are also highly effective in the purification of wastewater from water-soluble toxic hydrophilic compounds such as metal ions and organic dye. The functionalization with hydrophobic molecules can improve the purification of wastewater from organic waste,[21] while an amphiphilic nature of the adsorbent would allow targeting a broader range of pollutants.

On these bases, in this study a new approach is proposed to functionalize biopolymers with fluorinated aromatic heterocycles under mild reaction conditions, conferring an amphiphilic surface to the polymers. The modification of CE and CMC was achieved by reaction with 3-pentadecafluoroheptyl-5-perfluorophenyl-1,2,4-oxadiazole (FOX), a fluorinated heterocycle able to undergo a nucleophilic aromatic substitution,[22] leading to fluoro-functionalization through a stable covalent bond with the biopolymeric framework (**Scheme 1**).

The functionalized biopolymers were characterized with X-ray photoelectron spectroscopy (XPS), differential scanning calorimetry (DSC), thermal gravimetric analysis (TGA), infrared

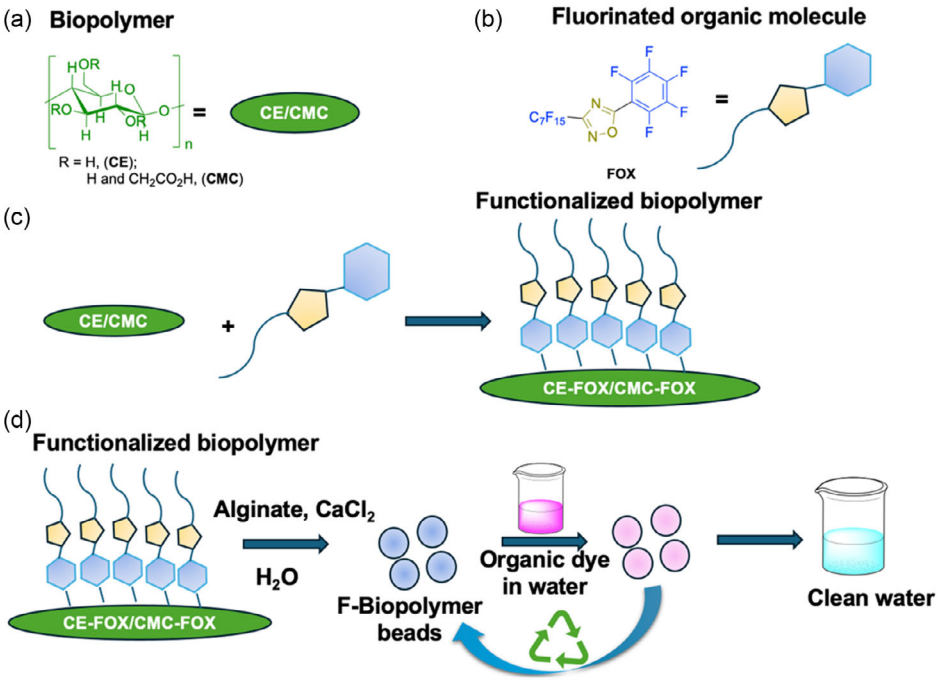

Scheme 1. Schematic representation of: a) structure of CE or CMC, b) structure of 3-pentadecafluoroheptyl-5-perfluorophenyl-1,2,4-oxadiazole (FOX), c) biopolymers functionalization reaction, and d) formation of alginate hydrogel-beads filled with functionalized biopolymers and their use as adsorbents for dye removal from wastewater.

spectroscopy, and scanning electron microscopy equipped with energy dispersive X-ray analysis (SEM-EDX). To test the amphiphilicity of the materials, water and oil contact angle measurements were performed. Being confident of the biocompatibility properties of other FOX-functionalized materials,[22,23] fluoro-functionalized biopolymers were then incorporated into sodium alginate hydrogel beads (SA)[24] to test the adsorption of dyes from wastewater as proof of concept of perspective applications in environmental remediation (Scheme 1d). For this purpose, a common cationic dye, RhB was used as model organic pollutant of wastewater. Bead morphology was analyzed through polarized optical microscopy (POM). Comparisons among adsorption tests with pure alginate beads, biopolymers, and fluoro-functionalized biopolymer beads were carried out. Adsorption tests were performed as function of time, as well as varying experimental conditions, such as mass of beads used as adsorbents. Furthermore, after dye adsorption, beads can quickly and easily desorb the pollutant in ethanol, allowing their recycling and reuse. The success of polymer functionalization and the consequent increase in adsorption ability opens new scenarios in the use of fluorinated biopolymers also as potential adsorbents of emerging pollutants.

2. Results and Discussion

2.1. Cellulosic Material Fluoro-Functionalization

FOX was synthesized as previously reported,[23a,25] then the biopolymers were functionalized through aromatic nucleophilic substitution as shown in **Scheme 2**. A strong base such as potassium *t*-butoxide was used to deprotonate polymer hydroxyl groups and push the nucleophilic attack.[22] Scheme 2 depicts the functionalization of CE or CMC with FOX occurring in 24 h, at room temperature, under mild conditions.

2.2. Functionalized Biopolymers Characterization

2.2.1. Infrared Spectroscopy (FTIR/ATR)

FTIR analysis was performed to assess structural changes following covalent functionalization of cellulosic substrates with FOX. However, interpreting the results (**Figure 1**a) proved challenging. FOX molecules exhibit more IR bands compared to CE and CMC. After functionalization, the hybrid materials also demonstrated increased IR activity in agreement with the presence of FOX in the cellulosic material.

Two of the most prominent signals of FOX molecules, specifically the peak at 1497 cm^{-1} attributed to C═C stretching in the aromatic ring of the perfluorophenyl group and the signal at 833 cm^{-1} likely due to C—F stretching in perfluorinated segments, were lost after functionalization (see magenta arrows in the plot). This observation aligns with previous findings where the attachment of FOX onto graphene oxide (GO) and GO-silica (GOS) similarly resulted in signal loss,[22,23] suggesting an analogous behavior.

Nevertheless, remaining modes within the 1300–850 cm^{-1} range (C—O/C—F region) and below 750 cm^{-1} are somehow still discernible, although combined with those of cellulosic materials. A close-up of spectral features in the 1300–850 cm^{-1} range is provided in Figure 1b, since the analysis of this region is useful to reveal the presence of fluorinated moieties and potential changes in C—O signals, indicative of alkyl-aryl ether formation.

Several characteristic modes of FOX are still identifiable in CE-FOX and CMC-FOX, albeit overlapped with typical cellulose signals. Notably, peaks associated with C—F stretching vibrations of perfluoroalkyl chains and the perfluorophenyl group (1201 cm^{-1}, 1153 cm^{-1}, 1145 cm^{-1}, 1131 cm^{-1}, 1107 cm^{-1}, 1096 cm^{-1}, labeled as ω_1-ω_6) remain visible, as well as those labeled as ω_7–ω_{10}: 1037 cm^{-1} (C—O stretching in the oxadiazole ring), 1020 cm^{-1} (mix of C—O and C—F stretching), 1010 cm^{-1} (C—F stretching), and 991 cm^{-1} (C—F out-of-plane bending in the aromatic ring).

Interestingly, after functionalization, the bands centered at 969 cm^{-1} (ω_{11}) and 931 cm^{-1} (ω_{12}) were no longer detectable. These modes, respectively assigned to out-of-plane bending or skeletal vibrations specific to the oxadiazole ring and to specific C—F stretching or bending vibrations, may also suggest successful functionalization, with new ether bonds or other interactions altering the original vibrational profile of FOX molecules.

Aiming to evaluate the contribution of asymmetric ═C—*O*—C stretching, the spectral range 1270–1230 cm^{-1} was multi-peak fitted by means of Gaussian curves and the results are provided in Figure 1c–d. In CE-FOX (Figure 1c), the intensity of the mode

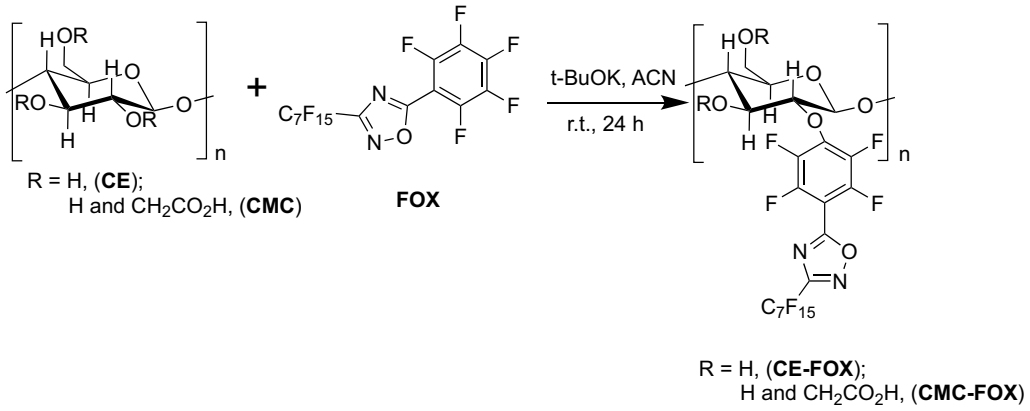

Scheme 2. Reaction scheme of CE and CMC functionalization reaction.

Research Article
doi.org/10.1002/ejoc.202500035

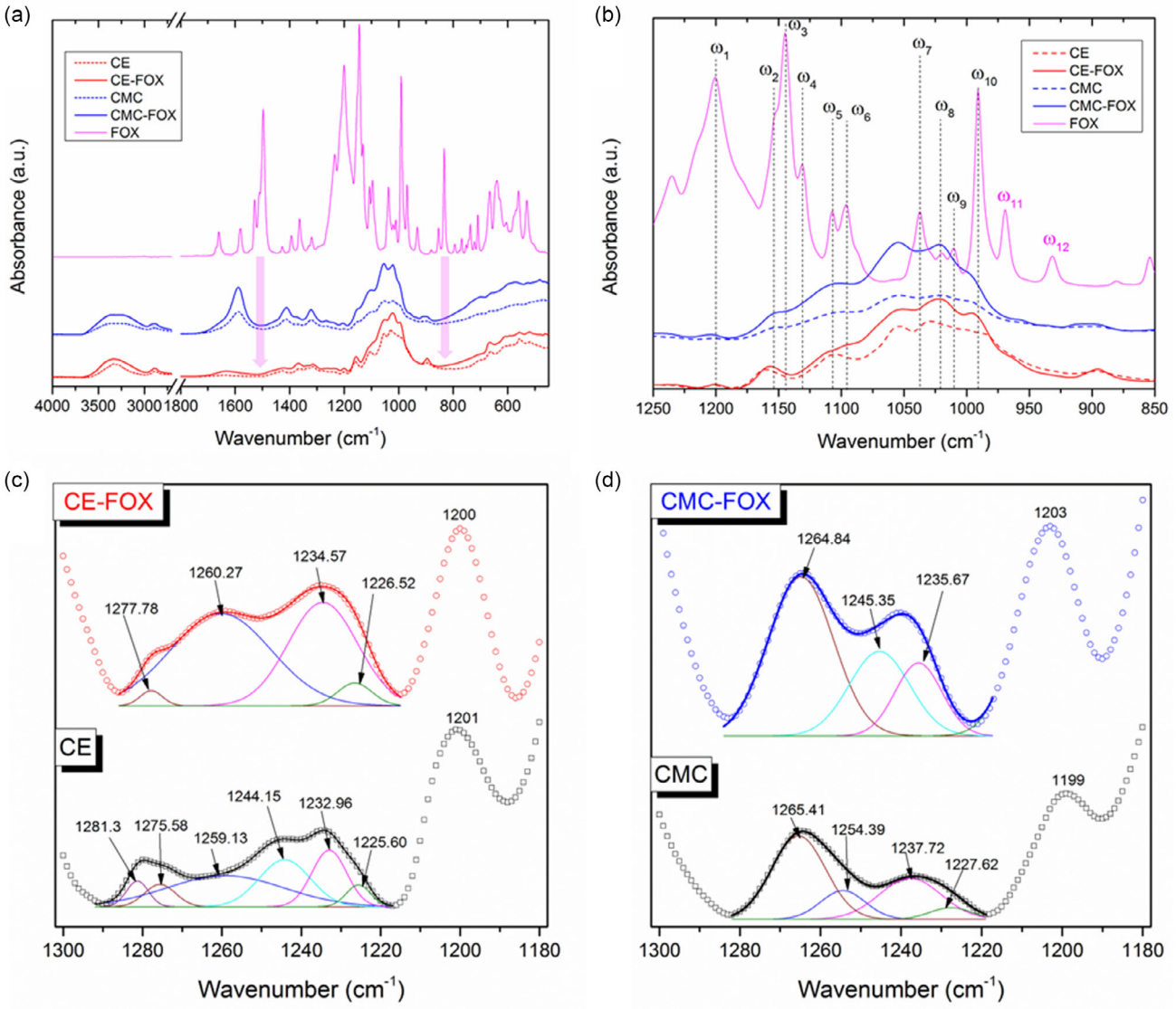

Figure 1. FTIR analysis: a) full-range spectra of the samples; b) and close-up of 1250–850 cm^{-1} spectral region. Multi-peak fitting in the range 1280–1220 cm^{-1} for: c) CE and CE-FOX; d) CMC and CMC-FOX samples.

centered at 1260 cm^{-1} increased after functionalization, while the modes at 1281 and 1244 cm^{-1} disappeared, and all the signals showed changes in wavenumber and intensity. In CMC and CMC-FOX (Figure 1d), the intensity of modes centered at 1265 and 1235 cm^{-1} displayed a significant increase, while the signal at 1228 cm^{-1}, typical of CMC, was no longer detectable in CMC-FOX. Conversely, CMC-FOX exhibited a new band, located at 1245 cm^{-1}.

2.2.2. X-Ray Photoelectron Spectroscopy (XPS)

XPS spectroscopy was performed on CE-FOX and CMC-FOX. Both samples showed peaks distinctive for C, O, N, F, and K, whose abundance (expressed as percentage values) is reported in **Table 1**. The presence of K likely derived from the synthetic procedure used to obtain the polymers, and it was more pronounced for CMC-FOX than CE-FOX. Besides, both materials displayed N and F peaks, corroborating the polysaccharide functionalization with FOX. Specifically, CMC-FOX featured higher N and F percentage values than CE-FOX, suggesting a greater functionalization of the former polysaccharide.

High-resolution C1 and F1 spectra of both samples were subsequently deconvoluted to establish the different C and F

Table 1. Elemental composition and abundance obtained for CE-FOX and CMC-FOX from XPS spectra.

Element	CE-FOX(%)	CMC-FOX(%)	CE(%)	CMC(%)	FOX(%)[a)]
C	47.8	22.9	53.1	66.0	40.5
N	2.5	7.10	–	–	5.4
O	23.3	13.5	46.9	29.5	2.7
F	29.4	39.1	–	–	51.4
K	3.10	17.3	–	–	–

[a)]from reference[23a]

species within these polymers, which are displayed and assigned in **Figure 2**a–d.

As a result, both FOX-functionalized polysaccharides showed the same C-containing species deriving from both cellulosic moieties (284.8–288 eV)[14] and fluorinated compounds (289.0–294 eV),[14,26] alongside K $2p_{1/2}$ and $_{3/2}$ signals in the 293–296 eV range.[27] Regardless of the similarities of C1 spectra, the abundance of C-containing species (expressed as percentage values) differed between the functionalized polysaccharides (Figure 2e), reflecting their different chemical structure and functionalization degree. In this regard, CE-FOX showed an elevated percentage for C—O groups, whereas the highest CMC-FOX value was observed for C—C sp^3 species, aligning with the chemical structure of cellulose and CMC. Moreover, the general higher abundance of cellulosic moieties inferred that, although FOX functionalized both polysaccharides, their retention of hydrophobic

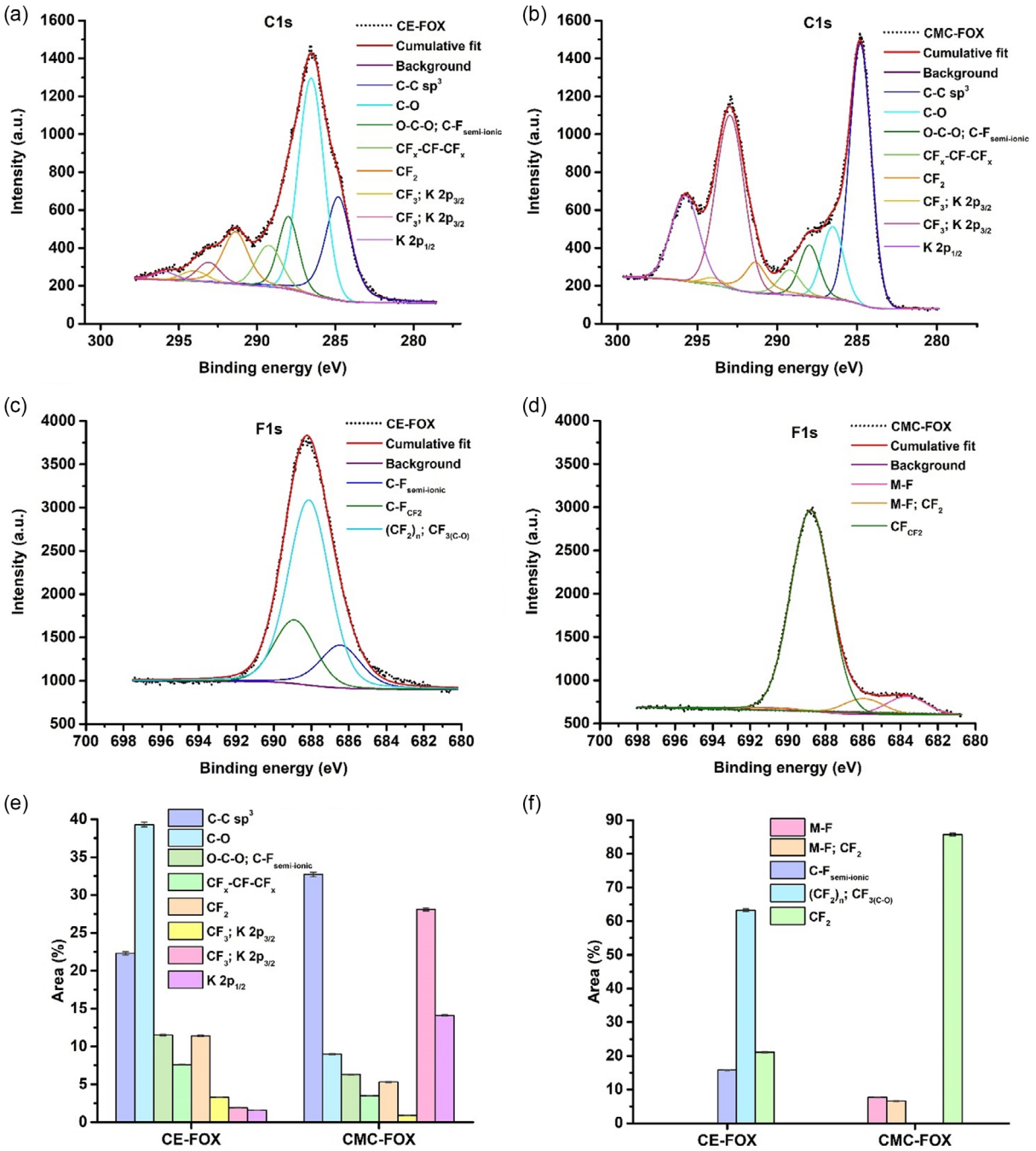

Figure 2. High-resolution XPS spectra of a,b) carbon (C1s) and c,d) fluorine (F1s) acquired for (a–c) CE-FOX and (b,d) CMC-FOX. Binding energies for (a,b) C1s: C—C sp^3 (cellulose) bonds at 284.8 eV, C—O (cellulose) bonds at 286.5 eV, O—C—O (cellulose) and semi-ionic C—F bonds at 288.0 eV, C—F (CF_x—CF—CF_x) bonds at 289.3 eV, CF_2 bonds at 291.3 eV, CF_3 bonds and K $2p_{3/2}$ signal at 293.1–294 eV, and K $2p_{1/2}$ signal at 296 eV. Binding energies for (c,d) F1s: metal (M)—F bonds at 683.7 and 686 eV (CMC-FOX), CF_2 bonds at 686 (CMC-FOX), semi-ionic C—F bonds at 686.5 eV (CE-FOX), CF_2 bonds of fluorinated chains and/or CF_3 bonds within CO-containing molecules at 688.2 eV (CEFOX), and CF_2 bonds at 688.9 eV. The distribution, expressed as area, of carbon and fluorine species is represented in panels e) and f), respectively.

C—F groups is limited. The distribution of CF-containing species resulted similar for both polymers, with semi-ionic C—F and CF_2 groups more represented than those referring to $(CF)_x$ chains.[14,26] Semi-ionic C—F bonds typically form between graphite, graphene, reduced graphene, or carbon-containing substrates, and fluorinated compounds,[28] so probably the presence of these species in functionalized biopolymers can be indicative of the occurrence of CE and CMC functionalization with FOX. Moreover, the strength of this interaction can vary depending on the nature of the C/F interaction, which corresponds to changes in the binding energy of these bonds,[28] even though CE-FOX and CMC-FOX revealed the same peak centered at 288 eV referring to semi-ionic C—F bonds. The high-resolution F1 spectra showed higher variability than the C1 ones, suggesting that multiple processes and interactions involving fluorine atoms can occur in both polymers. Indeed, CMC-FOX featured F1 peaks attributed to metal-fluorine (*M*-F) interactions (683.7–686 eV),[29] likely deriving from the conspicuous amount of K (17.1%) observed for this sample. On the contrary, the semi-ionic C—F binding energy of 686.5 eV was detected in CE-FOX, aligning with the results of C1 spectra. Besides, this polymer showed a high contribution at 688.2 eV that can relate to CF_2 bonds within fluorinated chains or CF_3 bonds within molecules containing C—O groups, [29b,30]that is, cellulose. The greatest F1 peak for CMC-FOX referred to C—F bonds with CF_2 moieties as first neighbors (688.9 eV),[31] which was present, even though in small quantity, within CE-FOX. Overall, XPS spectroscopy confirmed the functionalization of CE and CMC with FOX, underlying differences pertaining to the interactions involving fluorinated moieties of the latter with these polysaccharides.

To have further insights in the functionalization process, the elemental analysis of pristine and functionalized materials was carried out by XPS analysis. The degree of surface functionalization (X) was estimated according to Equation (1), expressing F of functionalized material in respect to the ones of FOX.

$$X_F = F\%_{\text{functionalized polymer}}/F\%_{FOX} \quad (1)$$

where the subscript F stands for fluorine atomic percentage used to measure the extent of functionalization.[23a] X_F indicated a degree of functionalization of ≈50% for CE-FOX and ≈70% for CMC-FOX. Values of functionalization are only indicative of a good degree of functionalization of the materials as K signals, evidencing also K–F interactions, complicate the analysis.

2.2.3. Thermal Analysis

Thermal analysis of pure FOX, pure and functionalized biopolymers has been carried out through DSC and TGA. DSC and TGA traces are shown in **Figure 3**.

DSC trace of FOX shows the endothermic peak during the heating process ascribable to the melting temperature at 38.97 °C and the crystallization temperature in the cooling cycle at 18.14 °C (Figure 3a). While biopolymer DSC traces show two endothermic events during the heating cycle and no events in the cooling one. Considering the enthalpies associated with the processes and the lack of crystallization, the first peaks were ascribed to the polymer melting temperature and the second ones to the polymer degradation temperature. Thermal behavior of CE and CMC drastically depends on the crystallinity and water content of samples.[32]

In all cases, different thermal events occurred in the functionalized polymers in respect to pure components, indicating the effective chemical functionalization of the materials. Furthermore, there is no peak of FOX melting or crystallizing in any of the curves, leading to the conclusion that the materials are covalently functionalized.

CE shows T_m at 167.15 °C and T_d 271.32 °C (**Table 2**), while a clear shift to lower temperatures for both events occurred for CE-FOX that melted at 141.66 °C and degraded at 203.28 °C. Lower T_m and T_d values can be very useful for the processability of the material, and it was previously observed also for some fluorinated esters of cellulose.[13] On the contrary, CMC-FOX shows slightly higher values than CMC (147.13 °C, 185.16 °C, T_m and T_d for pure CMC and 154.22, 199.36 °C T_m and T_d for CMC-FOX).

A more accurate analysis of degradation temperatures of the materials was carried out by TGA (Figure 3d). A gradual decrease of T_d can be observed for functionalized materials presenting also two degradation events during the heating process instead of one as in the case of pure biopolymers. In general, T_d are different from the ones of pristine biopolymers and FOX, confirming the functionalization of the biopolymers.

2.2.4. Morphology of Functionalized Cellulosic Material

The morphological characterization of the samples was carried via scanning electron microscopy (SEM) and is reported in **Figure 4** and **5**

SEM micrographs of CE and CE-FOX samples, provided in Figure 4, show the heterogeneous nature of microparticles in terms of both geometry and dimensions, which is substantially retained even after functionalization. No significant changes could be detected following chemical modification, although a slight increase in surface roughness was observed for CE-FOX, consistently with previously reported literature.[14]

In contrast, the comparison between SEM micrographs of CMC and CMC-FOX samples (Figure 5) reveals significant changes imparted by functionalization. Raw CMC particles can be regarded as spongy microtubes, with micrometric pores and a rough texture, having diameters between 10 and 20 μm and lengths varying in the range of 100–600 μm.

Surprisingly, CMC-FOX displays a completely different morphology, becoming much more similar to graphene oxide-based aerogels.[33] This sample, in fact, is characterized by self-assembled sheets, presumably arising from the opening of microtubes along a cutting line. Notably, the CMC-FOX foils exhibit an extremely smoother texture, with the absence of pores and holes. These surprising outcomes could be explained by considering that the hydrophobic interactions occurring after FOX-grafting somehow surpassed the hydrophilic ones due to the oxygenated moieties of CMC. This led to the longitudinal unzipping of microtubes, which in turn evolved into thin 2D thin foils.

Research Article
doi.org/10.1002/ejoc.202500035

Chemistry Europe
European Chemical Societies Publishing

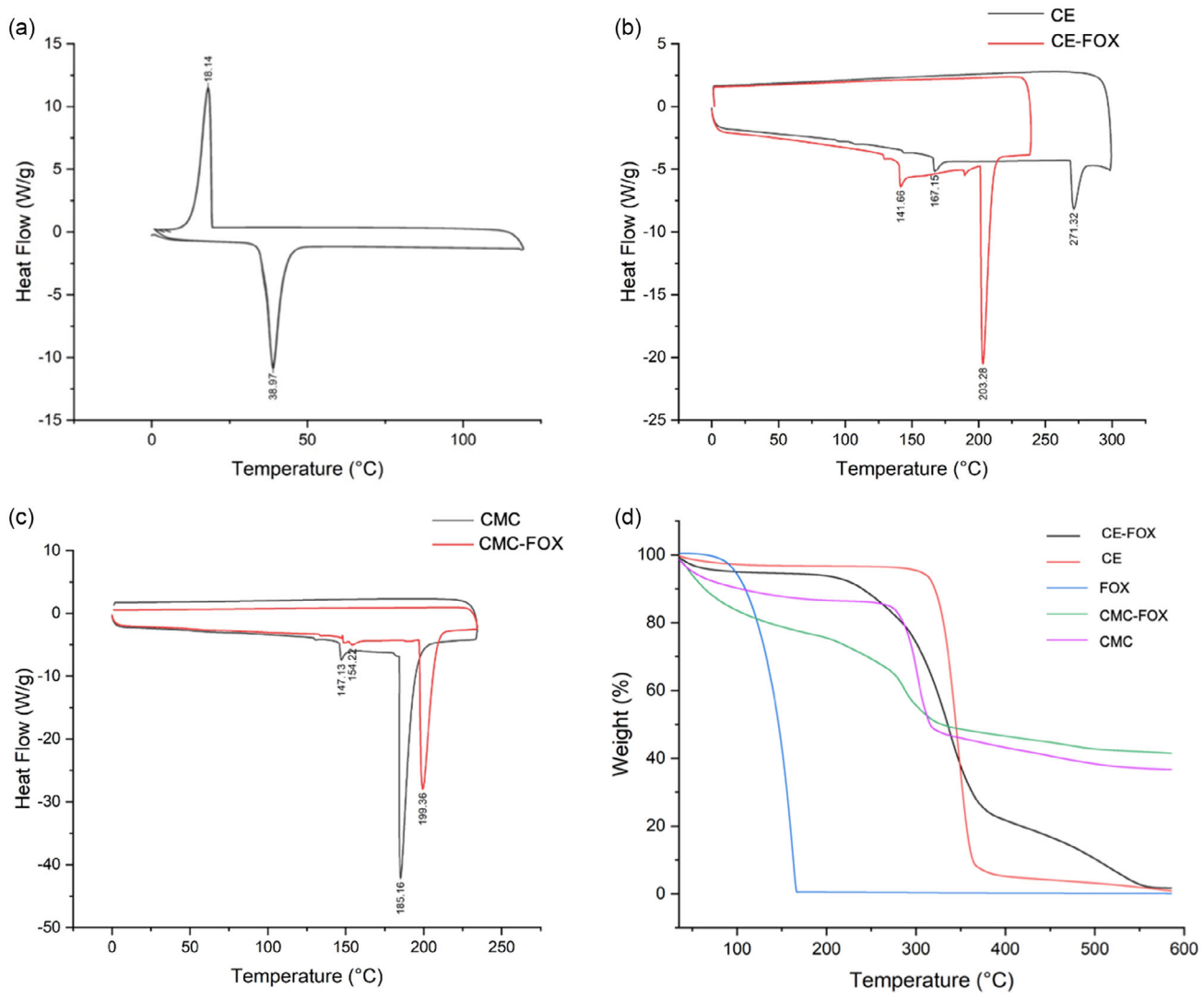

Figure 3. DSC traces of a) FOX, b) CE and CE-FOX, c) CMC, and CMC-FOX. Exothermic peaks point upward, d) TGA traces of pristine and functionalized cellulosic materials.

Table 2. Melting temperatures (T_m), degradation temperatures (T_d) and corresponding enthalpies (ΔH_d) of FOX and biopolymers obtained from DSC traces; degradation temperatures (T_d) determined by TGA.

	T_m [°C]	ΔH_m [J g^{-1}]	T_d [°C] [DSC]	ΔH_d (J [g]$^{-1}$) [DSC]	T_d [°C] [TGA]
FOX	38.9	49.6	–	–	161
CE	167.2	5.6	271.3	17.3	348
CE-FOX	141.7	5.3	203.3	86.1	226, 336
CMC	147.1	8.1	185.2	213.5	300
CMC-FOX	154.2	8.9	199.4	172.8	215, 283

Surprisingly, the functionalization of CMC with FOX led to the formation of smooth sheets, while for some fluorinated films derived from cellulose, a higher roughness was previously observed.[13,14] To the best of our knowledge, the successful preparation of 2D cellulose materials has never been reported before, and it could be revolutionary in many application fields.

EDX analysis performed on large areas of the samples was performed to qualitatively assess the presence and distribution of some key elements confirming XPS analysis, namely C, O, N, Na, K, and F (Figure S1–S4, Supporting Information).

Fluorine was detected only in the FOX-functionalized samples and it was more evidently mapped in CMC-FOX than in CE-FOX.

2.2.5. Water and Oil Contact Angle Measurements

A homogenous film of CMC-FOX was obtained by room temperature pressing to perform water contact angle (WCA) and oil contact angle (OCA) measurements. **Figure 6**b provides the trend of WCA and OCA as a function of time, along with some representative images of the droplet acquired during the experiments of OCA (top panels, Figure 6a) and WCA (bottom panels, Figure 6c).

As illustrated in the plot, the CMC-FOX film exhibits a superhydrophilic surface, with an initial WCA of 10.58°, which rapidly decreases to zero within a few seconds. Notably, this hybrid

Research Article
doi.org/10.1002/ejoc.202500035

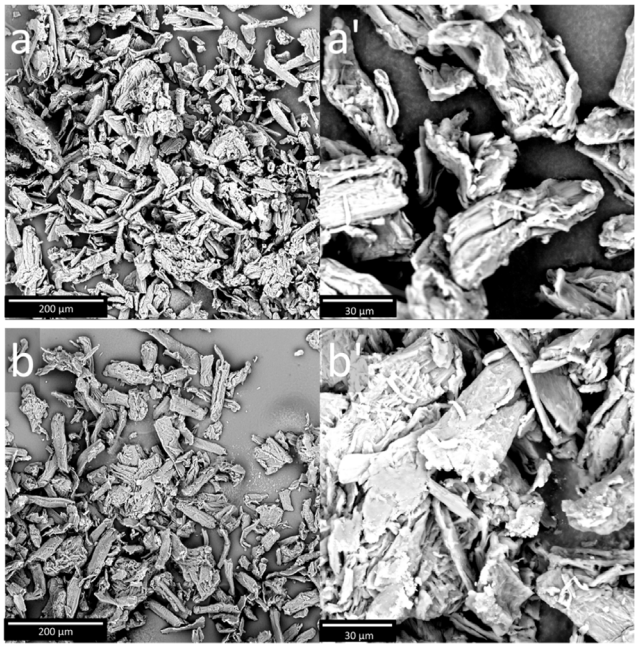

Figure 4. SEM micrographs at different magnifications of a-a') CE and b-b') CE-FOX microparticles.

material also demonstrates significant lipophilicity, with OCA decreasing from 69° to 60° over 100 s. This behavior indicates that the CMC-FOX retains the hydrophilic properties of CMC while the presence of fluorinated tails imparts amphiphilic characteristics to the material. A similar behavior was observed for some zwitterionic poly (fluoroaryl ether oxadiazole) ultrafiltration membranes exhibiting good antifouling and antibacterial properties.[17] Therefore, unlike the typical behavior of fluorinated branched cellulose films, which generally become hydrophobic,[13] the unique morphology and surface chemistry resulting from the combination of FOX and CMC produces amphiphilic materials. These materials could hold significant potential in the field of water treatment.

2.3. Testing Fluorinated Cellulosic Material as Adsorbents for Dye Removal

2.3.1. Incorporation of Biopolymers in SA Hydrogel Beads

Adsorption process can be more efficient with a semisolid adsorbent rather than a powder that would be more difficult to remove from the depurated water. Hence, pure and functionalized CE and CMC were incorporated into sodium alginate hydrogel beads (SA).[34] It is well known that when mixed with water, alginate forms a viscous gel, crosslinking the alginate chains with metal ions, like Ca^{2+}, which harden the hydrogel. The hydrogel works as a matrix that can include none to several other biopolymer-based materials to influence properties of the hydrogel, keeping SA biocompatibility.[24,35] The simplest structures are beads, but more complex objects have also been realized through 3D printing with a special alginate-based ink.[37c] In addition, carbon nanomaterials can be added to increase the adsorption efficiency of semisolid matrices.[36]

So, hydrogel beads were prepared by dissolving or dispersing biopolymers in water, SA was then added to the mixture to obtain a homogeneous gel with 1:1 ratio SA/biopolymer. The gel was added dropwise into a stirred solution of 1 wt% $CaCl_2$ in water,[37] after 30 min of hardening and calcium saturation, beads were obtained and dried at room temperature for 4 h before use (Figure S5, Supporting Information). Functionalized hydrogel beads obtained proved to be stable over 1 year from preparation.

Morphological investigation of SA hydro-beads with pure and functionalized biopolymers was carried out with polaryzed optical microscopy (POM) as the integral bead can be observed without removal of water as needed for SEM analysis.

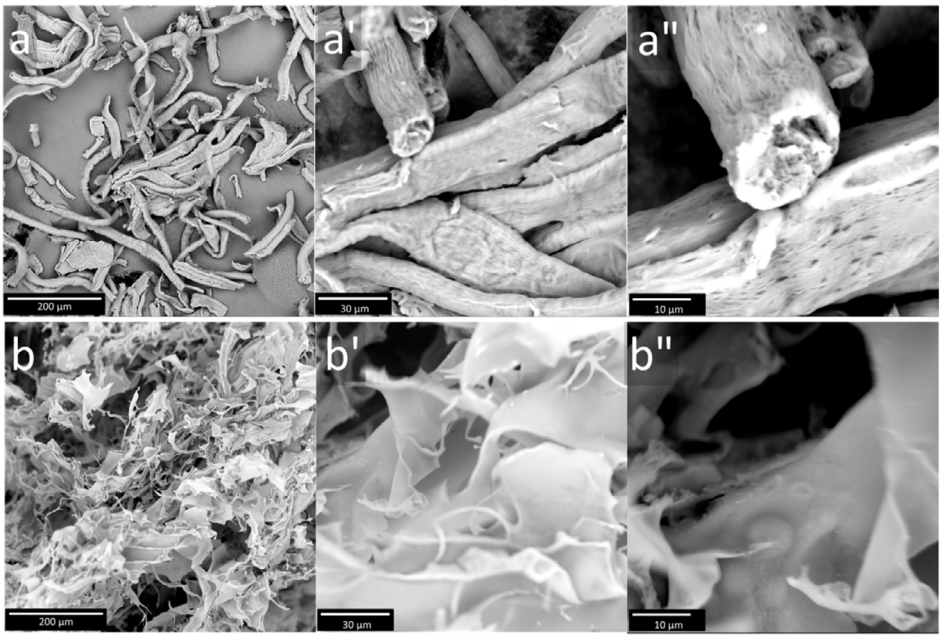

Figure 5. SEM micrographs at different magnification of a-a") CMC and b-b") CMC-FOX.

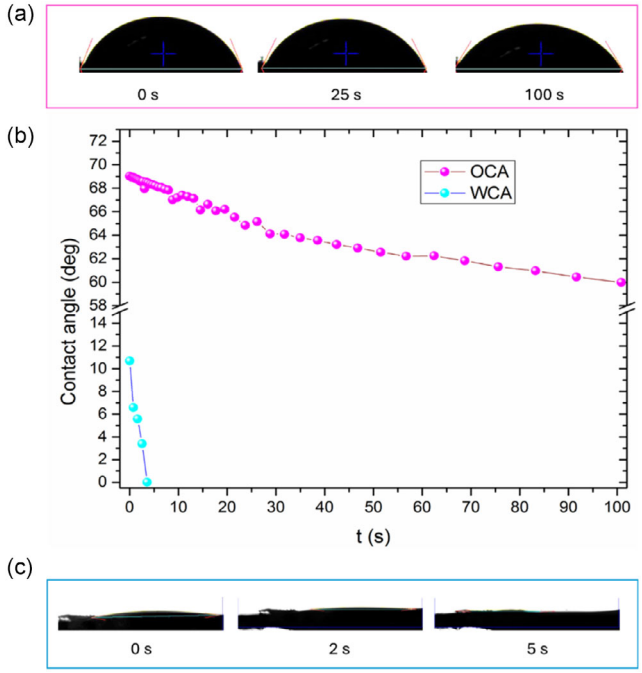

Figure 6. Wettability of CMC-FOX film: WCA and OCA as a function of time b), along with images captured at given times during WCA (bottom, c) and OCA (top, a).

SA/CE beads show a fibrous morphology as expected,[37] without any birefringence on polarized light (Figure S6a, Supporting Information) while SA/CE-FOX ones show fibers reflecting polarized light (Figure S6b, Supporting Information), indicating the presence of fluorine functionalization. On the other hand, comparing SA/CMC and SA/CMC-FOX morphologies (Figure S6c–d, Supporting Information), a denser structure with a more wrinkled and rougher surface can be observed for SA/CMC-FOX beads, which could increase the space for contact with the adsorbate, as previously reported.[38]

2.3.2. Adsorption Tests

Hydrogel beads were immersed in a water solution of RhB (2×10^{-5} M). RhB concentration was monitored by UV-vis spectroscopy at its absorbance maximum band (554 nm). The adsorbent material efficiency (E%) was calculated according to Equation (22) and RhB concentration was determined through a calibration curve. The absorbance decrease of RhB UV band (**Figure 7**a) was indicative of the dye adsorption in the beads and it can also be observed from the color change of the beads after contact with RhB solution (Figure 7b and S5b, Supporting Information).

A first screening of materials E% was carried out by immersing different beads in RhB solution for 24 h. Significant E% were obtained only for functionalized biopolymer beads (Figure 7c and S5b, Supporting Information), indicating that the presence of CE-FOX or CMC-FOX in the core of the beads is needed to efficiently remove organic molecules from wastewater. Hence, biopolymer functionalization led to a three-fold increase in efficiency (from 15% to 48%) for SA/CE-FOX and to an eight-fold increase in efficiency (from 11% to 94%) for SA/CMC-FOX (Table S1, Supporting Information). This trend indicates that the higher fluorine functionalization on biopolymer surface of CMC-FOX, observed with XPS and EDX measurements, favors the adsorption process. This is probably also due to the planar morphology of CMC-FOX sheets that warranties a higher area/volume ratio than in the case of CE-FOX. These data further support the effective functionalization of biopolymers, giving rise to a more lipophilic surface of the materials. According to literature, heterogeneous adsorption is governed by surface adsorption and diffusivity. These features are influenced by morphological parameters, such as pore volume and dimensions, surface specific area, and the availability of active sites. Additionally, physicochemical aspects like the wettability of the structures and the nature and extent of electrostatic or π–π interactions between the adsorbent and adsorbate also play a crucial role.[39]

Considering low RhB adsorption efficiency observed with pristine CE and CMC, it can be hypothesized that adsorption mechanism would occur thanks to the presence of FOX in biopolymers. RhB adsorption can be governed by combined interactions with CMC-FOX, including π−π stacking between aromatic ring of RhB and perfluoroaromatic heterocycle of FOX and electrostatic interactions between negatively charged CMC and cationic dye, as depicted in **Figure 8**. This mechanism

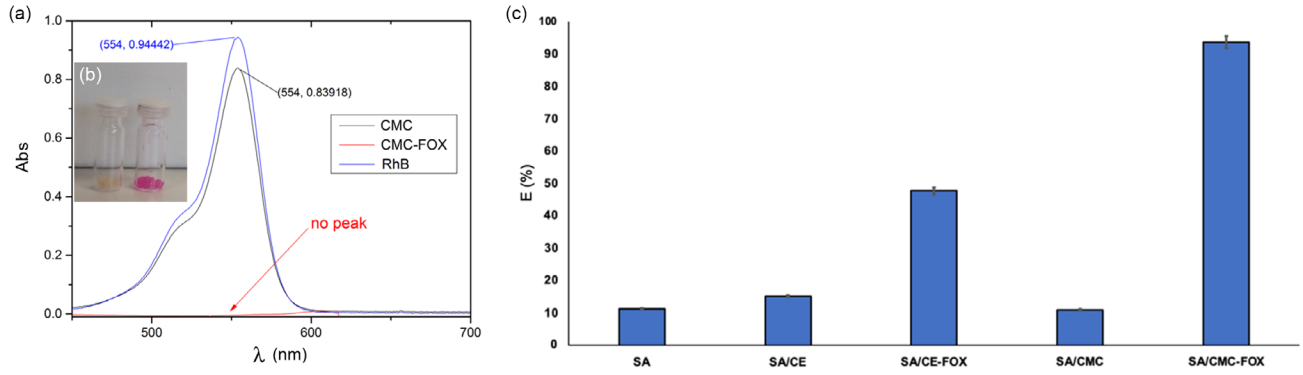

Figure 7. a) Spectra of RhB water solution at 2×10^{-5} M, before (blue line) and after 24 h of contact with SA/CMC (black line) and SA/CMC-FOX beads (red line); b) image of SA/CMC-FOX beads before and after adsorption; c) E% of different beads after 24 h of contact with RhB water solution at 2×10^{-5} M. E % is based on triplicate runs.

Research Article
doi.org/10.1002/ejoc.202500035

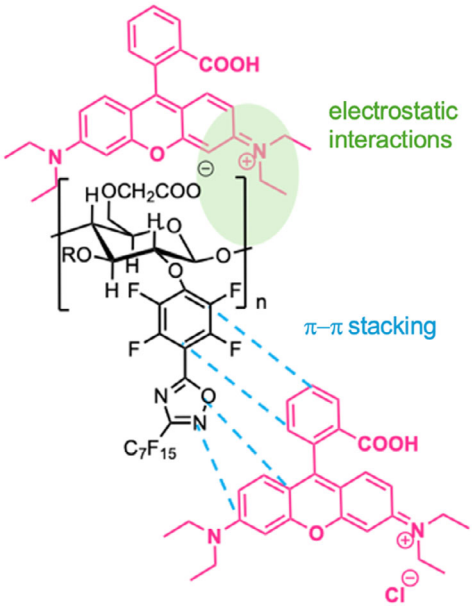

Figure 8. Schematic representation of possible interactions occurring among functionalized polymers and RhB.

is in line with previously observed selective dye adsorption mechanism in functionalized cellulose nanocrystals showing synergistic binding interactions, such as electrostatic attraction, π–π stacking, and hydrogen bonding.[40]

Encouraged by these preliminary tests, further adsorption experiments were performed by changing some experimental parameters. The best performing beads, that is, SA/CMC-FOX ones, were used as a model system. E% increased with the amounts of beads, revealing that a mass of 150 mg of beads is needed in 1.5 mL of dye solution to reach maximum E% in 24 h (Figure S7 and Table S2, Supporting Information).

Adsorption of RhB into SA/CMC-FOX beads was also studied as a function of time and it was expressed as E (%), according to Equation (2). **Figure 9** shows the trend obtained.

A gradual increase of E% can be observed in the first hours of contact between beads and RhB solution, reaching the plateau region in 18 h and the maximum value of 94%.

2.3.3. Maximum Loading and Recycling Tests

For the recycling and reuse of the adsorbents, two approaches were tested: i) reuse of beads without desorption (maximum loading test) and ii) washing and reuse of the beads. In the first case, after the first cycle of dye adsorption, the same beads were contacted with a new RhB solution (of the same concentration as the one used in the first cycle) for 24 h and these subsequent cycles were repeated to assess the residual E% after each loading cycle.

The beads, which showed an initial removal efficiency of nearly 90% in the second and third cycles of loading, showed a drastically decreased E% of 25% (Table S3, Supporting Information), demonstrating that adsorption sites of the beads were subjected to saturation starting from the third cycle.

In the second approach, the beads were first washed with ethanol to desorb the dye adsorbed through the previous cycle and the E% was assessed through the same loading method.

The desorption tests revealed that beads desorbed nearly 80% of the dye in 45 min with pure ethanol, and after a second desorption cycle, the beads were almost fully desorbed (**Figure 10**b). Desorption efficiency was evaluated following UV band of RhB. The beads were then washed with distilled water to remove excess ethanol and could then be reused for the subsequent adsorption test.

Therefore, a different scenario can be observed when the recycling test is performed after the desorption of dye from beads. Indeed, in most cases, a drop in efficiency is already reported after the fifth cycle of recycling of the adsorbent material,[24,38] while, in our case, beads could be recycled up to seven cycles, keeping E% $>$ 50% for all tested cycles (Figure 10a).

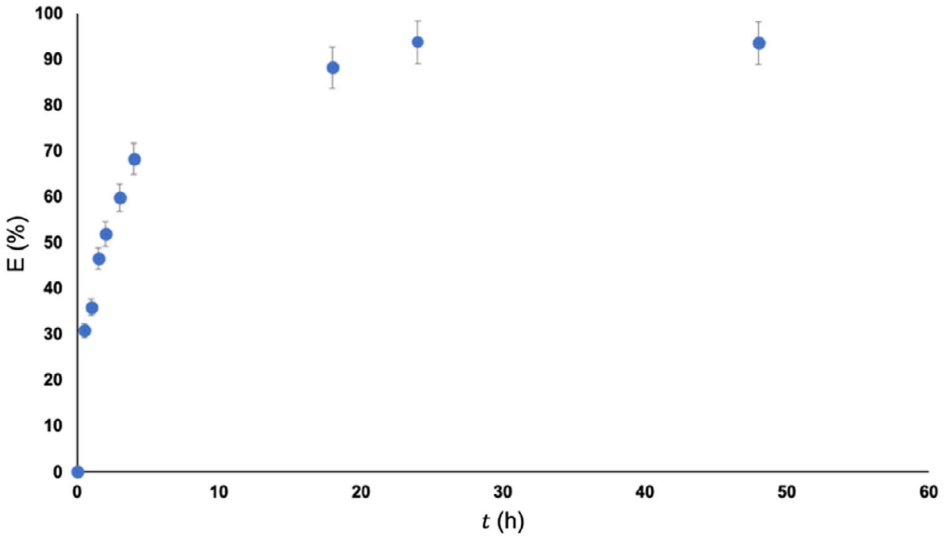

Figure 9. E% as function of time of contact with RhB water solution at 2×10^{-5} M. E% is based on triplicate runs.

Research Article
doi.org/10.1002/ejoc.202500035

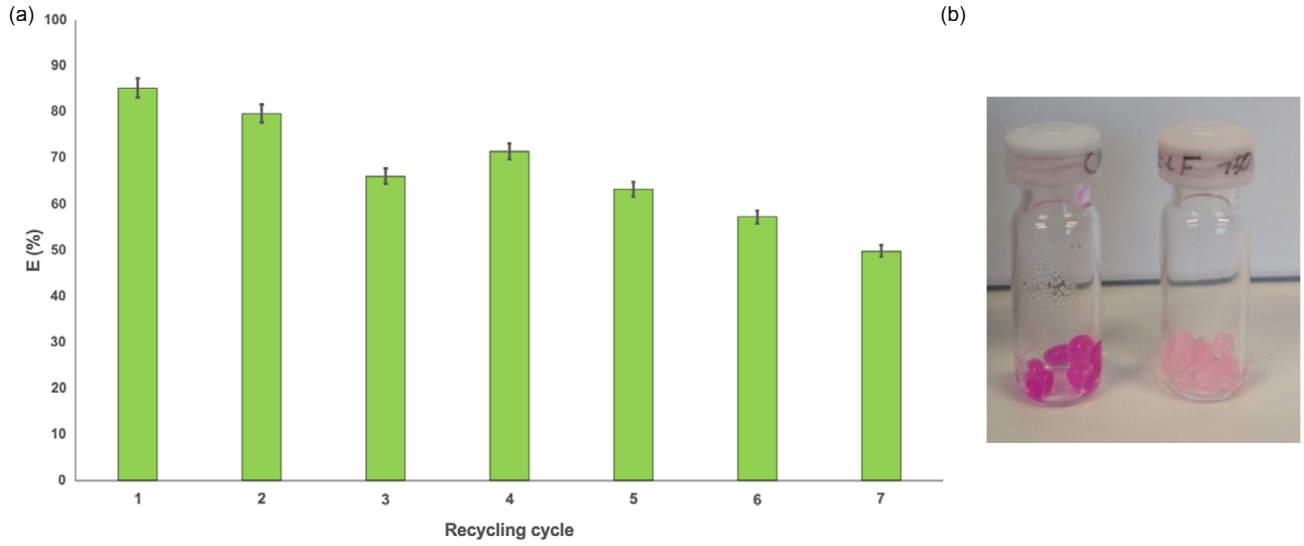

Figure 10. a) E% of SA/CMC-FOX beads after cycles of desorption and adsorption of dye. E % is based on triplicate runs; b) photo of beads before and after desorption of RhB with ethanol.

3. Conclusions

An easy functionalization of CE and CMC with fluorine-containing organic molecules was achieved under mild conditions. This process yielded biopolymers with amphiphilic surfaces due to the covalent attachment of 3-pentadecafluoroheptyl-5-perfluorophenyl-1,2,4-oxadiazole molecules, as confirmed by combined characterization techniques (FTIR/ATR, XPS, DSC, TGA, SEM-EDX). XPS analysis confirmed the presence of both the peculiar elements of the FOX molecules (N, F) in the functionalized materials, revealing higher functionalization for CMC-FOX than for CE-FOX. Both XPS and FTIR/ATR verified that the functionalization occurs via nucleophilic aromatic substitution, giving rise to new alkyl-aryl ethers. DSC clearly indicated different endothermic peaks compared to neat biopolymers, while TGA demonstrated distinct thermal events for functionalized biopolymers. SEM analysis showed higher surface roughness in the fiber morphology of CE-FOX. Interestingly, CMC-FOX exhibited unzipping of CMC microtubes, evolving into thin 2D foils, likely due to the increase in hydrophobic domains on the surfaces.

This study extends the strategies available for the fluorofunctionalization of biopolymers in order to gradually replace oil-derived fluoropolymers. The amphiphilic nature of the polymers enables their use in various applications, including as adsorbents for wastewater pollutants. As proof of concept, a practical application of functionalized biopolymers was explored. To simplify the adsorption process, CE-FOX and CMC-FOX were incorporated into alginate beads, which were immersed in dye water solutions. The results demonstrated an enhanced adsorption ability of functionalized polymers compared to the unfunctionalized ones, further validating the functionalization strategy. Finally, functionalized beads can be recycled for several cycles due to efficient desorption and adsorption processes.

This approach paves the way for the development of new fluorine-modified polymers as alternatives to fossil-based fluoropolymers, offering enhanced properties for a wealth of novel applications.

4. Experimental Section

Materials

Acetone, acetonitrile, silica, anhydrous calcium chloride, diethyl ether, ethanol, ethyl acetate, hydroxylamine hydrochloride, LC-grade water, pentafluorobenzoyl chloride, perfluorooctanonitrile, petroleum ether, potassium carbonate, potassium *t*-butoxide, pyridine, Rhodamine B, sodium alginate, sodium bicarbonate, microcrystalline cellulose, sodium carboxymethylcellulose, sodium hydroxide, sodium sulfate, and toluene was purchased from commercial sources and used without any further purification. 3-Pentadecafluoro-5-pentafluoroheptyl-1,2,4-oxadiazoles (FOX) was synthesized as previously reported.[23a,25]

Methods: Synthesis of Fluoro-Functionalized Cellulosic Material

100 mg of microcrystalline CE or CMC were sonicated in acetonitrile (8 mL) for 10 min. Then, potassium *t*-butoxide (300 mg) was added, and the mixture was stirred for 15 min and FOX (200 mg) was finally added. The reaction was carried out for 24 h of constant stirring at room temperature, monitoring FOX presence in the mixture through thin-layer chromatography. After that time, the reaction solvent was evaporated, and then the residue was transferred into a Falcon tube. Washings with water (3 × 10 mL) and then ethyl acetate (3 × 10 mL) by centrifugation (4000 rpm) and removal of the supernatant were carried out. The solid residue was dried through lyophilization.

For CMC functionalization, similar conditions were used, but after the water washings, the wet gelatinous sediment needed to be lyophilized before washing with ethyl acetate.

Methods: Attenuated Total Reflection Fourier Transform Infrared (FTIR/ATR) Spectroscopy

FTIR/ATR spectroscopy was performed using a Perkin-Elmer FT-IR/NIR Spectrum 400 spectrophotometer. The spectra were recorded in the range 4000–450 cm^{-1}.

Methods: XPS

XPS was performed as previously described.[41] Briefly, PHI5000 VersaProbe II Scanning XPS Microprobe (ULVAC-PHI) working with an Al (Al $K_\alpha = 1486.6$ eV) anode was used. The beam was focused to a diameter of 200 μm (50 W) using Ar^+ and e^- charge neutralization and a 45° electron take-off angle. C1s and F1s high resolution (0.1 eV) XPS spectra were collected, and the XPSPEAK v4.0 software was used to analyze the spectra through a nonlinear least-square fitting procedure to identify different C and F species.

Methods: Differential Scanning Calorimetry (DSC)

DSC measurements were carried out with a TA Instruments mod. 2920 Differential Scanning Calorimeter (TA Instrument Inc., New Castle, DE, USA) equipped with a TA Instruments Refrigerated Cooling System. Samples (≈4 mg) were weighed in aluminum TA Tzero Hermetic Pans, which were subsequently sealed with aluminum lids. The analysis was performed with heating and cooling rates of 20 °C min^{-1} under a N_2 atmosphere of 50 mL min^{-1}. Three heating and cooling ramps were carried out in a temperature range between 0 °C and 300 °C depending on the material.

Methods: Thermogravimetric Analysis (TGA)

TGA was performed by using the TGA 550 Discovery Series (TA Instruments) apparatus under nitrogen flow, which was 60 cm^3 min^{-1} for the sample and 40 cm^3 min^{-1} for the balance. The samples were weighted, with mass ranging from 1 to 4 mg, and heated from room temperature up to 600 °C with a scanning rate of 20 °C min^{-1}.

Methods: Scanning Electron Microscopy (SEM)

The morphology of the samples was investigated via SEM imaging, carried out with a Phenom ProX instrument (Thermo Fisher Scientific, USA), equipped with a probe for energy dispersive X-ray (EDX) analysis.

Methods: Water and Oil Contact Angle (WCA and OCA)

WCA and OCA testing were performed at room temperature using an FTA 1000 instrument (First Ten Ångstroms, UK). A 4 μL drop of either deionized water or motor oil was dispensed onto the sample surface via an automatic liquid drop dosing system. Images of the droplet on the surface were acquired at various time intervals, ranging from 0 (at the moment of contact) to 100 s.

Methods: SA Beads Preparation

SA/polymers beads were prepared by modifying a previously reported procedure.[37] Beads with a 1:1 (w/w) ratio of sodium alginate (SA) and biopolymer were prepared. In particular, the biopolymer (15 mg) was added to LC-grade water (1 mL) and stirred for 5 to 10 min. Then, SA (15 mg) was slowly added in small portions while the mixture was vigorously stirred for 15 min. The obtained gel was then added dropwise into a stirred solution of 1 wt% aqueous $CaCl_2$ (20 mL). After 30 min of hardening and calcium saturation, the beads were filtered and washed three times with distilled water and left to dry in open air and at room temperature for 4 h.

Methods: Polarized Optical Microscopy (POM)

A POM analysis of beads was performed on a Zeiss Axio imager. A2m microscope (Carl Zeiss, Göttingen, Germany) equipped with a Linkham hot-stage LTS420E with a Linkpad T95-LTS processor to control the temperature. The samples were placed between a glass slide and a cover slip. An Axiocam ICC1 digital camera mounted atop the microscope was used to collect photomicrographs. Images were recorded at magnifications of 5x, 10x, or 20x and in cross-polarized light.

Methods: Dye Adsorption Tests

To evaluate the adsorption capacities of the obtained material, 150 mg of each type of beads was weighed into a vial and 1.5 mL of aqueous RhB solution (2×10^{-5} M) was added. After 24 h, the supernatant solution was collected and analyzed by UV. The amount of RhB adsorbed by the bead is expressed as adsorption efficiency (*E*%) according to the following equation (2)[42]

$$E\% = \frac{c_0 - c_t}{c_0} \cdot 100\% \quad (2)$$

In which c_0(mol L^{-1}) is the initial concentration, and c_t (mol L^{-1}) the concentration after the specified time of contact with the beads.

The RhB concentration is measured spectrophotometrically, spectra were recorded on a Specord S600 (Analytik Jena). RhB presents a maximum of absorption at 554 nm and concentrations were determined based on calibration curve, this last obtained by measuring the absorbance of standard aqueous solutions of the dye in the following concentration range: 3.2×10^{-6}–3.2×10^{-5} M.

Methods: Dye Adsorption Kinetics

To evaluate the dye adsorption kinetics on the beads, a stock solution (2×10^{-5} M) of RhB was prepared by dissolving an appropriate amount of the dye in LC-grade water. A unique batch of SA/CMC-FOX hydrogel beads was prepared, from which several aliquots were weighed (≈75 mg) in different vials (1.5 mL) and put in contact with 0.75 mL of adsorbate solution. The adsorption of the adsorbate was studied over various time intervals ranging from 0.5 to 48 h. At each specified time point, 0.5 mL of the solution was withdrawn and diluted in LC-grade water to measure the absorbance at UV spectrophotometer.

Methods: Maximum Loading and Recycling Tests

Maximum loading tests were performed on the most performing adsorbent material (SA/CMC-FOX beads). 75 mg of the beads were contacted with a RhB solution (2×10^{-5} M) for 24 h (first loading cycle). Loaded beads were then isolated by removing the initial RhB solution and contacted again with a freshly prepared RhB solution (0.75 mL, 2×10^{-5} M) for the subsequent 24 h (second loading cycle). This procedure was repeated without washing the beads until a significant decrease in E% (E% $< 30\%$) was reached.

Recyclability tests were performed on beads that underwent the first loading cycle (75 mg of SA/CMC-FOX beads contacted for 24 h with 0.75 mL of a 2×10^{-5} M RhB solution) by previously desorbing the RhB dye. Desorption tests were performed using EtOH (2×1.5 mL $\times$ 45 min). After desorption, beads were isolated from the EtOH solution and washed with water for 16 h and then immersed in a fresh RhB solution (0.75 mL, 2×10^{-5} M) for the subsequent 24 h. This procedure was repeated until E % decreased below 50%.

Acknowledgements

This work was supported by the Italian Ministry of Education, University, and Research (MUR) through the National

Operational Program (PON) Project on Research and Innovation 2014–2020 (Azione IV.v – Contratti di ricerca su tematiche dell'Innovazione – B75F21002190001). The authors thank ATeN Center at the University of Palermo and Dr. Michelangelo Scopelliti for XPS experiments. They thank Prof. Giuseppe Lazzara for TGA facilities.

This study was carried out within the MICS (Made in Italy—circular and Sustainable) Extended Partnership and received funding from the European Union Next-GenerationEU (PIANO NAZIONALE DI RIPRESA E RESILIENZA (PNRR) -MISSIONE 4 COMPONENTE 2, INVESTIMENTO 1.3 -D.D. 1551.11-10-2022, PE00000004).

C.R. thanks PNR next generation EU-DM737/2021-CUP B79J21038330001 and FFR2023 granted by Università degli Studi di Palermo for funding. SAMOTHRACE (Sicilian micro and nano technology research and innovation center) extended partnership and received funding from the European Union Next-GenerationEU (PIANO NAZIONALE DI RIPRESA E RESILIENZA (PNRR) – MISSIONE 4 COMPONENTE 2, INVESTIMENTO 1.5).

This manuscript reflects only the authors' views and opinions, neither the European Union nor the European Commission can be considered responsible for them.

Open access publishing facilitated by Universita degli Studi di Palermo, as part of the Wiley–CRUI–CARE agreement.

Conflict of Interest

The authors declare no conflict of interest.

Author Contributions

Davide Ricci: data curation (equal); investigation (equal); formal analysis (equal). **Andrea Maio**: data curation (equal); formal analysis (equal); investigation (equal); writing—review & editing (equal). **Christian Jahns**: Investigation (supporting). **Elena Piacenza**: formal analysis (supporting). **Delia Francesca Chillura Martino**: validation (equal); visualization (equal). **Roberto Scaffaro**: validation (equal); visualization (equal). **Margit Schulze**: visualization (equal). **Andrea Pace**: validation (equal); writing—review & editing (equal). **Carla Rizzo**: conceptualization (equal); funding acquisition (equal); methodology (equal); writing—original draft (lead); writing—review & editing (equal). **Ivana Pibiri**: conceptualization (equal); supervision (equal); resources (equal); writing—review & editing (equal). **Davide Ricci** and **Andrea Maio** contributed equally to this work.

Data Availability Statement

The data that support the findings of this study are available from the corresponding author upon reasonable request.

Keywords: cellulose · environmental remediation · fluorinated molecules · functionalized biopolymers · wastewater pollution

[1] a) C. Xia, H. Ye, Y. Wu, H. A. L. Garalleh, M. Garaleh, A. Sharma, A. Pugazhendhi, *Chemosphere* **2023**, *314*, 137663; b) M. Zubair, A. Ullah in *Chapter 14 - Biopolymers in environmental applications: industrial wastewater treatment*, Eds.: S. Thomas, S. Gopi, A. Amalraj), Elsevier, Amsterdam **2021**, pp. 331–349; c) P. R. Yaashikaa, P. Senthil Kumar, S. Karishma, *Environ. Res.* **2022**, *212*, 113114; d) C. Rizzo, G. Misia, S. Marullo, F. Billeci, F. D'Anna, *Green Chem.* **2022**, *24*, 1318.

[2] a) V. Dichiarante, M. I. Martinez Espinoza, L. Gazzera, M. Vuckovac, M. Latikka, G. Cavallo, G. Raffaini, R. Oropesa-Nuñez, C. Canale, S. Dante, S. Marras, R. Carzino, M. Prato, R. H. A. Ras, P. Metrangolo, *ACS Sustain. Chem. Eng.* **2018**, *6*, 9734; b) W. Song, L. Qian, Z. Miao, V. Nica, Y. Zhao, Z. He, Y. Zhu, J. Gao, X. Li, *Carbohydr. Polym.* **2023**, *315*, 121001.

[3] N. Hernández, R. C. Williams, E. W. Cochran, *Org. Biomol. Chem.* **2014**, *12*, 2834.

[4] D. Klemm, B. Heublein, H.-P. Fink, A. Bohn, *Angew. Chem. Int. Ed.* **2005**, *44*, 3358.

[5] C. F. Liu, R. C. Sun, A. P. Zhang, J. L. Ren, X. A. Wang, M. H. Qin, Z. N. Chao, W. Luo, *Carbohydr. Res.* **2007**, *342*, 919.

[6] P. McNeice, G. H. ten Brink, U. Gran, L. Karlson, R. Edvinsson, B. L. Feringa, *RSC Sustain.* **2024**, *2*, 369.

[7] a) N. Verma, K. Pramanik, A. K. Singh, A. Biswas, *Mater. Technol.* **2022**, *37*, 706; b) S. Javanbakht, M. T. Nazeri, A. Shaabani, M. Ghorbani, *Int. J. Biol. Macromol.* **2020**, *164*, 2873; c) S. Bayarri, L. González-Tomás, E. Costell, *Food Hydrocoll.* **2009**, *23*, 441; d) A. A. P. Mansur, F. G. de Carvalho, R. L. Mansur, S. M. Carvalho, L. C. de Oliveira, H. S. Mansur, *Int. J. Biol. Macromol.* **2017**, *96*, 675.

[8] a) C. He, F. Wang, J. Kang, C. Lv, X. He, Z. Li, *Mater. Today Commun.* **2023**, *34*, 105082; b) C. Huang, Y. Gao, Y. Chen, Y. Shen, H.-Y. Yu, *J. Clean. Prod.* **2024**, *451*, 142107.

[9] a) K. Li, X. Zeng, H. Li, X. Lai, *Appl. Surf. Sci.* **2014**, *298*, 214; b) F. Ouhib, A. Dirani, A. Aqil, K. Glinel, B. Nysten, A. M. Jonas, C. Jerôme, C. Detrembleur, *Polym. Chem.* **2016**, *7*, 3998.

[10] S. Ebnesajjad, *Fluoroplastics: Non-melt processible fluoropolymers: The definitive user's guide and data book Plastics Design Library*, Elsevier, Amsterdam **2014**.

[11] N. Kaushal, A. K. Singh, *Int. J. Biol. Macromol.* **2023**, *246*, 125709.

[12] M. Le Gal, A. Rios De Anda, L. Michely, C. Simon Colin, E. Renard, V. Langlois, *Biomacromolecules* **2021**, *22*, 4510.

[13] G. Tedeschi, S. Guzman-Puyol, L. Ceseracciu, J. J. Benitez, L. Goldoni, A. Koschella, T. Heinze, G. Cavallo, V. Dichiarante, G. Terraneo, A. Athanassiou, P. Metrangolo, J. A. Heredia-Guerrero, *Carbohydr. Polym.* **2021**, *271*, 118031.

[14] A. Baidya, M. A. Ganayee, S. Jakka Ravindran, K. C. Tam, S. K. Das, R. H. A. Ras, T. Pradeep, *ACS Nano* **2017**, *11*, 11091.

[15] M. Ulbricht, *Polymer* **2006**, *47*, 2217.

[16] W. Gao, H. Liang, J. Ma, M. Han, Z.-l. Chen, Z.-s. Han, G.-b. Li, *Desalination* **2011**, *272*, 1.

[17] H. Guo, Z. Wang, Y. Liu, P. Huo, J. Gu, F. Zhao, *J. Membr. Sci.* **2020**, *611*, 118337.

[18] D. Park, C. J. Weinman, J. A. Finlay, B. R. Fletcher, M. Y. Paik, H. S. Sundaram, M. D. Dimitriou, K. E. Sohn, M. E. Callow, J. A. Callow, D. L. Handlin, C. L. Willis, D. A. Fischer, E. J. Kramer, C. K. Ober, *Langmuir* **2010**, *26*, 9772.

[19] S. Krishnan, C. J. Weinman, C. K. Ober, *J. Mater. Chem.* **2008**, *18*, 3405.

[20] F. Koschitzki, O. Özcan, R. Wanka, M. Krisam, A. Rosenhahn, *Adv. Mater. Interfaces* **2024**, *11*, 2400370.

[21] D. Bekchanov, M. Mukhamediev, S. Yarmanov, P. Lieberzeit, A. Mujahid, *Carbohydr. Polym.* **2024**, *323*, 121397.

[22] A. Maio, R. Scaffaro, L. Lentini, A. Palumbo Piccionello, I. Pibiri, *Chem. Eng. J.* **2018**, *334*, 54.

[23] a) A. Maio, D. Giallombardo, R. Scaffaro, A. Palumbo Piccionello, I. Pibiri, *RSC Adv.* **2016**, *6*, 46037; b) R. Di Gesù, A. Palumbo Piccionello, G. Vitale, S. Buscemi, S. Panzavolta, M. F. Di Filippo, A. Leonarda, M. Cuccia, A. Di Prima, R. Gottardi, *bioRxiv* **2025**, *17*, 025025.

[24] S. Thakur, B. Sharma, A. Verma, J. Chaudhary, S. Tamulevicius, V. K. Thakur, *J. Clean. Prod.* **2018**, *198*, 143.

[25] A. Palumbo Piccionello, A. Guarcello, A. Calabrese, I. Pibiri, A. Pace, S. Buscemi, *Org. Biomol. Chem.* **2012**, *10*, 3044.

[26] a) L. Jun, W. Qing, H.-C. Huang, J.-J. Chen, *Text. Res. J.* **2011**, *81*, 1702; b) Y.-G. Lei, K.-M. Ng, L.-T. Weng, C.-M. Chan, L. Li, *Surf. Interface Anal.* **2003**, *35*, 852; c) G. I. Semushkina, Y. V. Fedoseeva, A. A. Makarova, D. A. Smirnov, I. P. Asanov, D. V. Pinakov, G. N. Chekhova, A. V. Okotrub, L. G. Bulusheva, *Nanomaterials* **2022**, *12*, 231.

[27] a) L. Caracciolo, L. Madec, H. Martinez, *ACS Appl. Energy Mater.* **2021**, *4*, 11693; b) J.-H. Kim, G. Lee, J.-E. Park, S.-H. Kim, *Processes* **2021**, *9*, 1000.
[28] a) D. Claves, *New J. Chem.* **2011**, *35*, 2477; b) Y. Sato, K. Itoh, R. Hagiwara, T. Fukunaga, Y. Ito, *Carbon* **2004**, *42*, 3243.
[29] a) J. Choi, K.-d. Seong, J. Kang, M. Hwang, J. M. Kim, X. Jin, Y. Piao, *Electrochim. Acta* **2018**, *279*, 241; b) R. G. Haverkamp, *J. Mater. Sci.* **2012**, *47*, 1262.
[30] V. A. Shelestova, P. N. Grakovich, S. F. Zhandarov, *Compos. Interfaces* **2011**, *18*, 419.
[31] E. Durand, C. Labrugère, A. Tressaud, M. Renaud, *Plasmas and Polymers* **2002**, *7*, 311.
[32] L. Szcześniak, A. Rachocki, J. Tritt-Goc, *Cellulose* **2008**, *15*, 445.
[33] R. Scaffaro, A. Maio, F. Lopresti, D. Giallombardo, L. Botta, M. L. Bondì, S. Agnello, *Compos. Sci. Technol.* **2016**, *128*, 193.
[34] a) C. V. Flores, J. L. Obeso, H. Viltres, E. Torres-García, A. R. Rajabzadeh, S. Srinivasan, R. A. Peralta, I. A. Ibarra, C. Leyva, *RSC Sustain.* **2024**, *2*, 239; b) S. Morozkina, U. Strekalovskaya, A. Vanina, P. Snetkov, A. Krasichkov, V. Polyakova, M. Uspenskaya, *Polymers* **2022**, *14*, 3604; c) J. Yuan, C. Yi, H. Jiang, F. Liu, G. J. Cheng, *ACS Appl. Polym. Mater.* **2021**, *3*, 699.
[35] a) Z.-H. Hu, A. M. Omer, X. k. Ouyang, D. Yu, *Int. J. Biol. Macromol.* **2018**, *108*, 149; b) T. Wu, Y. Bu, X. Chen, J. Fan, Z. Yu, H. Yan, Q. Lin, *Colloids Surf., A* **2025**, *709*, 136154.
[36] a) T. Wang, W. Wang, C. Hu, J. Zheng, Z. Zhu, B. Liu, *Carbohydr. Polym.* **2024**, *342*, 122358; b) C. Rizzo, S. Marullo, F. D'Anna, *Environ. Sci.: Nano* **2021**, *8*, 131.
[37] T. H. A. Mai, V. N. Tran, V. V. M. Le, *Biochem. Eng. J.* **2013**, *74*, 81.
[38] H. Zhao, X.-K. Ouyang, L.-Y. Yang, *J. Mol. Liq.* **2021**, *324*, 115122.
[39] R. Scaffaro, A. Maio, M. Gammino, *Adv. Compos. Hybrid Mater.* **2024**, *7*, 13.
[40] N. Mohammed, H. Lian, M. S. Islam, M. Strong, Z. Shi, R. M. Berry, H.-Y. Yu, K. C. Tam, *Chem. Eng. J.* **2021**, *417*, 129237.
[41] E. Piacenza, F. Vitale, V. Ciaramitaro, R. Lombardo, F. Ferrante, D. F. Chillura Martino, *Mater. Today Chem.* **2024**, *38*, 102115.
[42] C. Rizzo, J. L. Andrews, J. W. Steed, F. D'Anna, *J. Colloid Interface Sci.* **2019**, *548*, 184.

Manuscript received: January 13, 2025
Revised manuscript received: March 20, 2025
Version of record online: